JOURNAL OF GEOPHYSICAL RESEARCH, VOL. 113, D14S09, doi:10.1029/2007JD009659, 2008

Click Here for Full Article

Laboratory investigation of fire radiative energy and smoke aerosol emissions

Charles Ichoku,[1,2] J. Vanderlei Martins,[2,3] Yoram J. Kaufman,[4,5] Martin J. Wooster,[6] Patrick H. Freeborn,[7,8] Wei Min Hao,[8] Stephen Baker,[8] Cecily A. Ryan,[8] and Bryce L. Nordgren[8]

Received 30 November 2007; revised 11 March 2008; accepted 28 March 2008; published 21 June 2008.

[1] Fuel biomass samples from southern Africa and the United States were burned in a laboratory combustion chamber while measuring the biomass consumption rate, the fire radiative energy (FRE) release rate (R_{fre}), and the smoke concentrations of carbon monoxide (CO), carbon dioxide (CO_2), and particulate matter (PM). The PM mass emission rate (R_{PM}) was quantified from aerosol optical thickness (AOT) derived from smoke extinction measurements using a custom-made laser transmissometer. The R_{PM} and R_{fre} time series for each fire were integrated to total PM mass and FRE, respectively, the ratio of which represents its FRE-based PM emission coefficient (C_e^{PM}). A strong correlation ($r^2 = 0.82$) was found between the total FRE and total PM mass, from which an average C_e^{PM} value of 0.03 kg MJ^{-1} was calculated. This value agrees with those derived similarly from satellite-borne measurements of R_{fre} and AOT acquired over large-scale wildfires.

Citation: Ichoku, C., J. V. Martins, Y. J. Kaufman, M. J. Wooster, P. H. Freeborn, W. M. Hao, S. Baker, C. A. Ryan, and B. L. Nordgren (2008), Laboratory investigation of fire radiative energy and smoke aerosol emissions, *J. Geophys. Res.*, *113*, D14S09, doi:10.1029/2007JD009659.

1. Introduction

[2] Biomass burning is a phenomenon that affects most vegetated landscapes around the world to various degrees and intensities. Some biomass fires originate by accident or from natural causes such as lightning, while others are deliberately ignited for agricultural, experimental, or litter control purposes. Landscape-scale vegetation fires can last anywhere from a few minutes to a few months and can burn areas ranging from a few square meters to thousands of square kilometers before they either burn out by themselves or are contained by various fire suppression techniques. Regardless of the origin, size, or duration of fire, one common feature of all biomass fires is the concomitant massive emission of smoke, which can be transported over distances ranging from a few to thousands of kilometers. This smoke is composed of aerosols or particulate matter (PM) and a large variety of trace gases (e.g., CO, CO_2, CH_4, nonmethane hydrocarbons, and other compounds). Here we focus on the emission of PM from biomass fires and use small-scale experiments to study this in the laboratory.

[3] Smoke PM can have tremendous impacts on human and animal health, air quality, visibility (affecting road and air transport), environmental sanitation, weather, and climate. Several studies have investigated some of these impacts [e.g., *DeBell et al.*, 2004; *Koren et al.*, 2004; *Procopio et al.*, 2004; *Feingold et al.*, 2005; *Kulkarni et al.*, 2005; *Liu* 2005; *McMeeking et al.*, 2006; *Wu et al.*, 2006]. However, the extent of these impacts cannot be fully determined unless emissions are accurately quantified in terms of PM emission rates from individual fires, as well as spatially and temporally aggregated total PM emissions from all fires occurring locally, regionally, or globally. It has long been recognized that the mass of any smoke constituent emitted by a fire is proportional to the mass of biomass burned [e.g., *Crutzen et al.*, 1979; *Crutzen and Andreae*, 1990, *Hao and Liu*, 1994]. Therefore, the traditional approach to estimate the mass emission of any particulate or gaseous species is to experimentally determine its typical mass emission factor (EF), which when multiplied by the burned biomass (BM) yields the mass of the emitted material [*Seiler and Crutzen*, 1980; *Andreae and Merlet*, 2001]. However, since it is often not possible to determine BM directly at the landscape scale, researchers have resorted to using various forms of data, including proxy information and statistics (such as population and

[1]Earth System Science Interdisciplinary Center, University of Maryland, College Park, Maryland, USA.
[2]Climate and Radiation Branch, NASA Goddard Space Flight Center, Greenbelt, Maryland, USA.
[3]Now at Department of Physics, University of Maryland, Baltimore County, Baltimore, Maryland, USA.
[4]Department of Physics, University of Maryland, Baltimore County, Baltimore, Maryland, USA.
[5]Deceased 31 May 2006.
[6]Department of Geography, King's College London, Strand, London, UK.
[7]Now at Department of Geography, King's College London, Strand, London, UK.
[8]Fire Sciences Laboratory, Rocky Mountain Research Station, USDA Forest Service, Missoula, Montana, USA.

Copyright 2008 by the American Geophysical Union.
0148-0227/08/2007JD009659$09.00

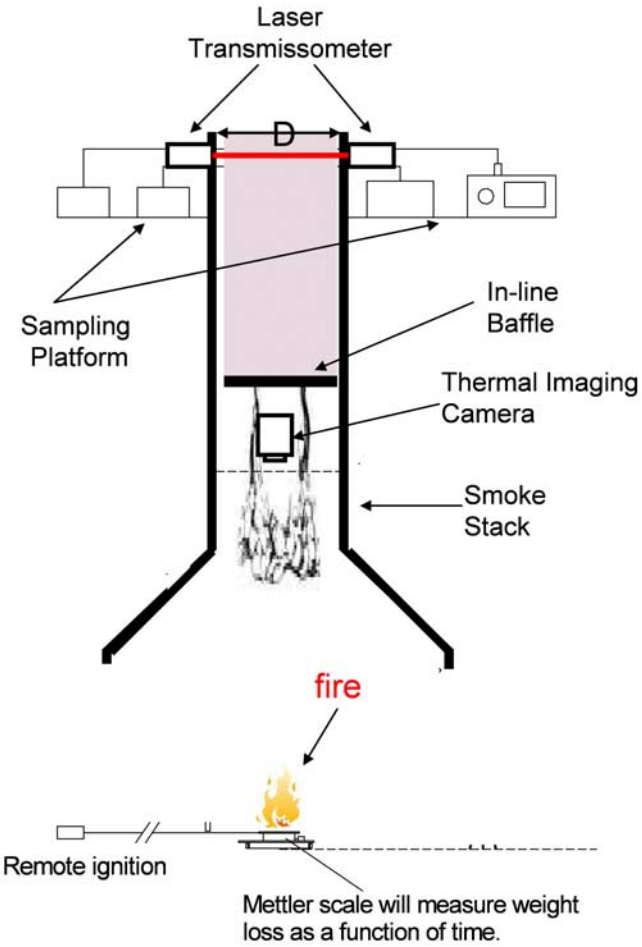

Figure 1. Combustion chamber burning arrangement showing the large smoke stack, beneath which fuel samples are placed on a Mettler scale and remotely ignited. The Agema 550 thermal imaging camera is suspended inside the smoke stack vertically above the fire to measure its thermal emission, which is used to derive the fire radiative power. An in-line baffle is located above the camera to ensure that the smoke is well mixed before it reaches the level of the elevated sampling/measurement platform where the laser transmissometer has been set up together with other smoke sampling and measurement instruments. This diagram is not drawn to scale.

agricultural practices) to derive estimates of BM. Such approximations result in considerable uncertainties in the derived emissions estimates of PM and trace gas species [*Andreae and Merlet*, 2001].

[4] Rapid developments in satellite technology during the last two decades have ushered in a new era in fire emissions estimation. Satellite remote sensing techniques now enable fire observations to be made regularly and routinely from space, thereby minimizing the danger, expense, and complexity associated with fire observation and measurement at close range [*Fuller*, 2000]. Importantly, it is the fire radiative energy (FRE), the radiant component of the total energy release from fires, that enables their detection from space in the first place. Therefore, seizing the advantage offered by this knowledge, a number of satellite sensors operational since 2000 have demonstrated the ability to measure the FRE rate of release (R_{fre}) or fire radiative power (FRP) [*Kaufman et al.*, 1996, 1998; *Wooster et al.*, 2003; *Roberts et al.*, 2005]. Although the measurement of thermal radiance is spectrally constrained by the bandpass of the sensor, and the calculation assumes an isotropic emitter, FRP (or R_{fre}) expresses a combination of the fire strength and size, which themselves are related to the rate of biomass consumption (R_{BM}). Indeed, a number of recent studies based on small-scale field experiments have clearly demonstrated a direct linear relationship between FRE and BM [*Wooster*, 2002; *Wooster et al.*, 2004, 2005]. Since FRE is related to BM, which in turn is related to emissions, it follows that FRE is itself related to emissions of PM and other species. On the basis of this assumption, *Ichoku and Kaufman* [2005] went on to use spaceborne measurements of R_{fre} and aerosol optical thickness (AOT or τ_a) to demonstrate a linear relationship between R_{fre} and the PM emission rate (R_{PM}) at the regional scale using measurements made by the Moderate Resolution Imaging Spectroradiometer (MODIS) sensor onboard the EOS Terra and Aqua satellites.

[5] The objective of the current study is to investigate the relationship between FRE and PM emissions at the laboratory scale, using a similar approach to the spaceborne methodology of *Ichoku and Kaufman* [2005] but with a closer view of the experimental conditions. The aim is to improve understanding of the fire energy/emissions mechanisms in order to facilitate a more in-depth interpretation of results obtained from spaceborne data sets. The ultimate aim is to reduce uncertainties associated with the estimation of PM emission at the landscape scale through application of a combined FRE and AOT approach.

2. Measurements

[6] This section describes (1) the general setup for the laboratory experiment, (2) the nature of the individual biomass-burning events studied, and (3) a special laser transmissometer designed specifically for this experiment to measure the smoke PM emission rate.

2.1. Experimental Setup

[7] The experiment was conducted in November 2003 in a combustion chamber located at the Fire Sciences Laboratory of the United States Forest Service Rocky Mountain Research Station in Missoula, Montana, United States. The experimental setup is described in detail by *Freeborn et al.* [2008] but will be summarized here for completeness. Inside the chamber, burns were conducted under a smoke stack in the form of an inverted funnel suspended above the ground, with its mouth located at a height of about 2 m above the chamber floor (see Figure 1). The stack's cylindrical part, which has an internal diameter of 1.52 m, extends up to a height of about 20 m. The chamber is not pressurized, but an induction fan located at the top of the stack enhances the flow of smoke up through it. To conduct a burn, the biomass fuel was arranged on a fire resistant ceramic plate placed on a weighing scale located approximately where the central axis of the stack meets the ground. A sand substrate was created on the plate before overlaying the biomass material in order to simulate the soil back-

Table 1. Measurements Conducted During the Experiment That Are Relevant to This Analysis[a]

Parameter	Units	Instrument
Biomass fuel mass	g	Mettler model PM34 digital scale
R_{fre} from thermal radiance Measurements at 3.9 μm wavelength	W	Agema 550 thermal imaging camera
Stack air flow velocity	m s^{-1}	Kurz model 455 hot wire anemometer
Carbon monoxide (CO) concentration	ppm	Thermo Environmental Instruments model 48C CO analyzer
Carbon dioxide (CO_2) concentration	ppm	Li-Cor model Li-6262 CO_2/H_2O analyzer
$PM_{2.5}$ total mass	g	gravimetric analysis of Teflon filter samples
Aerosol scattering coefficient at 450, 550, and 700 nm wavelengths	Mm^{-1}	TSI model 3563 three-wavelength integrating nephelometer
AOT from aerosol transmittance at 632 nm wavelength	unitless	laser transmissometer

[a]$PM_{2.5}$, particulate matter with aerodynamic diameter <2.5 μm; AOT, aerosol optical thickness.

ground of the vegetation in the landscape. While the fire is burning, the radiant heat emanating from it is measured at 3.9 μm with an Agema 550 imager suspended along the central axis of the stack at 5.4 m above the ground. This radiance measurement is later used to compute R_{fre}, on the basis of the method fully described by *Wooster et al.* [2005]. The smoke from the fire travels up the stack to a height of 16.54 m above ground, where it is sampled and measured by an array of gaseous- and particulate-sampling instruments operated from a suspended platform and connected to the same data logger as the biomass fuel weighing scale. There is an in-line baffle within the stack to ensure that the smoke is well mixed prior to sampling. This mechanical device therefore mixes up smoke probably emitted over a period of up to 10 s, which is a coarser temporal resolution than the sampling rate of each of the instruments, as will be discussed in section 3. A comprehensive list and details of all the measurements conducted during this experiment are given by *Freeborn et al.* [2008], but a selection of those measurements relevant to this discussion and their respective instrumentation is listed in Table 1. All the instruments used are standard commercially available instruments, with the exception of the laser transmissometer, which was designed and fabricated specifically for this experiment, as described in section 2.3.

2.2. Biomass Burning

[8] Different types of biomass fuel were collected for the experiment from southern Africa and the United States [*Freeborn et al.*, 2008]. Those relevant to the analysis performed here included ponderosa pine (*Pinus ponderosa,* hereinafter referred to as "Pipo") needles and branches less than 0.64 cm in diameter (i.e., 1 h fuel size class in the National Fire Danger Rating System), live herbaceous and woody Douglas fir foliage (*Pseudotsuga menziesii,* hereinafter referred to as "PsMe"), senesced grass collected from Zambian dambos and shredded aspen (*Populus* spp.) in the form of excelsior, and big sagebrush (*Artemisia tridentate,* hereinafter referred to as "sage"). Fuel was predried, and each burn was conducted with a sample of fuel initially weighing between 0.2 and 2.6 kg. Burns were conducted with both homogeneous and mixed fuels, and each sample was arranged on a fire resistant rectangular plate placed on a Mettler model PM 34 digital scale and ignited with a resistance coil. The fire starts at the point of ignition and spreads through the whole fuel pile. As the fire burned, the scale weighed the fuel sample to determine the rate of biomass loss (R_{BM}), the Agema 550 thermal infrared camera measured the spatially explicit spectral radiance to quantify the rate of release of FRE (R_{fre}), the transmissometer measured the smoke particulate transmittance for use in calculating the AOT and the PM emission rate (R_{PM}), and the remainder of the equipment located on the smoke-sampling platform measured other parameters relevant to the concentration and/or flux rate of smoke particulates and trace gases. Examples of such measurements include aerosol light scattering using a three-wavelength integrating nephelometer and the concentrations of carbon monoxide (CO) and carbon dioxide (CO_2). For reasons of conformity to the objectives of a different study involved in this experiment [*Freeborn et al.*, 2008], a 2.5 μm cut point cyclone was used at the nephelometer inlet, thereby restricting its measurement of scattering coefficients (σ_{sp}) to $PM_{2.5}$ (particulate matter with diameter less than 2.5 μm) size range. On the other hand, because of the open path length of the transmissometer, its measurements included all particle sizes. Therefore, given that $PM_{2.5}$ is self-explanatory, in this paper, all references to PM without subscript imply smoke aerosols of all sizes, also referred to as total PM (TPM) [e.g., *Andreae and Merlet*, 2001]. Indeed, this paper focuses on TPM emissions based on the transmissometer measurements, while other emissions ($PM_{2.5}$, CO, or CO_2) are used where necessary to support the analysis.

[9] There were 13 fires in which the transmissometer measurements coincided with the other measurements necessary for this analysis. Table 2 lists the fires and their corresponding fuel characteristics and fire duration, as well as their combustion and emissions results, which will be discussed in section 4. Since the experiment took place in November 2003, the fires are simply identified by date with a letter appended to indicate the order in the sequence of fires for that day, such that, for instance, the first fire conducted on 6 November 2003 is identified with 6A, and so on.

2.3. Laser Transmissometer

[10] The laser transmissometer was designed to measure the smoke laser transmittance, based upon which the smoke aerosol extinction optical thickness (AOT or τ_a) is calculated for use in estimating R_{PM}, the procedure of which will be described in section 3. The transmissometer comprises a laser source and a reference detector conveniently housed together in a small metal box, as well as a transmission detector housed in an identical box mounted across the smoke stack. A power supply adaptor is attached to each of the two boxes for connection to a power source. The laser reference and transmission detectors are both connected to a data logger, which is then connected to a computer for real-time graphic visualization of both the reference and transmitted signals as they are being logged. The "reference"

Table 2. Characteristics and Results of the Burns in Which the Transmissometer Was Involved[a,b]

1	2	3	4	5	6	7	8	9	10	11	12	13	14
Burn ID	Fuel Description	Mass Fraction (%)	Moisture Content (%)	Total Initial Mass (kg)	Burn Duration (s)	Burned Biomass (kg)	Total FRE (MJ)	Average Flow Rate (m s^{-1})	F_c (kg MJ^{-1})	TPM Emitted (g)	Ce: TPM (kg MJ^{-1})	$PM_{2.5}$ Emitted (g)	Ce: $PM_{2.5}$ (kg MJ^{-1})
6D	dambo grass (h)	100	5.30	0.57	2371	0.56	0.94	2.80	0.60	17.75	0.019	10.45	0.011
6E	dambo grass (h)	100	5.30	1.16	4762	1.13	1.47	2.57	0.77	71.38	0.049	24.85	0.017
7A	PiPo needles (1 h)[c]	44	7.49	0.31	2040	0.23	0.84	2.70	0.28	14.43	0.017	2.26	0.003
	PsMe foliage[d]	56	44.82										
7B	PiPo needles (1 h)[c]	24	7.49	0.52	2609	0.41	1.12	3.33	0.37	19.06	0.017	13.22	0.012
	PsMe foliage[d]	76	44.82										
7C	dambo grass (h)	100	6.34[e]	2.60	7914	2.51	3.42	3.17	0.74	113.64	0.033	35.64	0.010
7D	dambo grass (h)	100	6.34[e]	0.56	2791	0.56	1.05	3.28	0.53	37.74	0.036	20.07	0.019
7E	dambo grass (h)						0.75	3.15		4.79	0.006		
8A	dambo grass (v)	100					0.42	0.82					
8B	excelsior	100	5.92	0.85	5847	0.83	1.58	1.29	0.53			5.46	0.003
8C	sage	100	9.78	0.22	2119	0.19	0.68	1.30	0.28	15.73	0.023	6.97	0.010
8D	sage	100	9.78	0.22	2230	0.13	0.47	1.30	0.26	7.69	0.016		
8E	sage	100	9.78	0.20	2440	0.18	0.60	1.23	0.30	10.41	0.017	6.59	0.011
9A	PiPo needles (1 h)[c]	100	6.62	0.29		0.20	0.82	1.34	0.24	4.86	0.006		
9B	dambo grass (h)	100	6.34[e]				0.22	1.37		1.14	0.005		
9C	dambo grass (h)	100	6.34[e]				0.58	1.31		3.75	0.006		

[a]Vacant spaces simply mean that data are not available.
[b]ID, identification; F_c, fire radiative energy-based biomass combustion factor (i.e., BM/FRE); TPM, total particulate matter; C_e, FRE-based smoke emission coefficient (i.e., emitted smoke species/FRE); h, horizontal fuel arrangement; PiPo, *Pinus ponderosa*; PsMe, *Pseudotsuga menziesii*; v, vertical fuel arrangement.
[c]One hour fuel size class (i.e., diameter < 0.635 cm) based on the National Fire Danger Rating System.
[d]Live collected vegetation.
[e]Average moisture calculation.

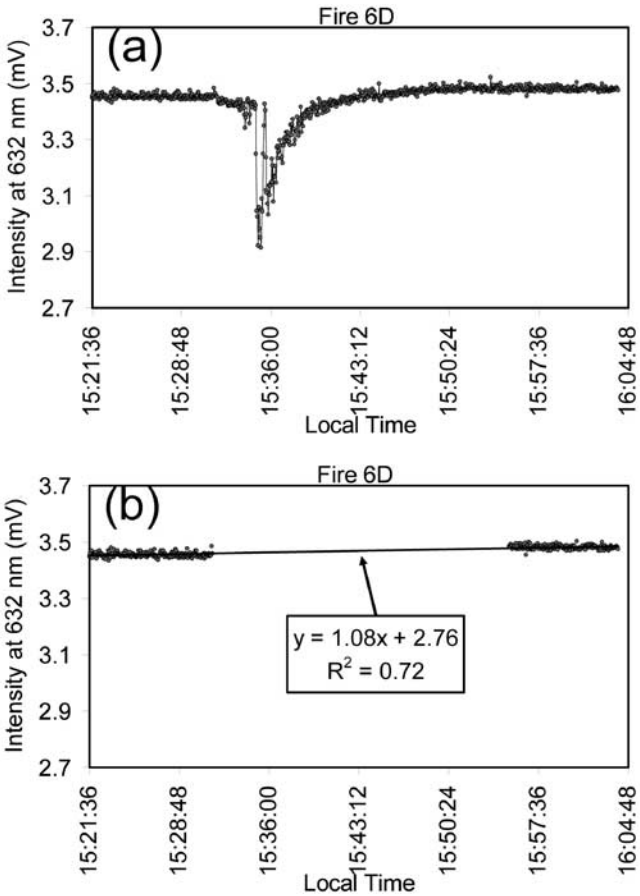

Figure 2. (a) Laser transmissometer measurement of a typical laboratory fire (in this case fire 6D), (b) segments of the measurements before and after the fire, with linear least squares fit used to determine the baseline of intensity for computing AOT.

signal is only used as a means of monitoring the stability of the laser source, while the measured "transmitted" signal will allow the degree of light attenuation by the smoke aerosol to be quantified.

[11] The smoke stack is equipped with access windows at the level of the smoke-sampling platform for setting up sampling equipment. Two of the access windows, located opposite each other across the diameter of the stack, were used to set up the transmissometer (see Figure 1). The laser source was designed to emit a collimated narrow laser beam (about 2 mm diameter, at 632 nm wavelength) pointed to the transmission detector as accurately as possible.

[12] The laser transmissometer measured the transmitted laser intensity (at 632 nm wavelength) across the smoke stack every 3 s. The AOT at 632 nm (or τ_{a632}) across the stack diameter for each data record was calculated using the following equation:

$$\tau_{a632} = -\ln(I/I_0), \tag{1}$$

where I is the intensity of the laser signal transmitted through the smoke, and I_0 the intensity when no smoke is present in the stack. I/I_0 is the measured smoke transmittance. The process used to obtain the values for I_0 was to start the transmissometer measurements well before a fire was lit and to continue well after it was over. Figure 2a shows the measurement time series for a typical fire. Under ideal conditions, if parts of the intensity data segments before and after the fire are extracted and fitted with a straight line, that line should be horizontal. However, during the current experiment, the line was often slightly inclined, probably because of a slow linear drift in laser alignment caused by temperature changes to its components and metal casing or vibration from movements on the platform. Therefore, I_0 cannot be assumed constant, but a least squares equation of the line is generated for use in interpolating the I_0 value corresponding to each measured I value recorded during the burn. Figure 2b illustrates the least squares linear fitting process on parts of the before-and-after data segments to derive the baseline equation for interpolating I_0 value for each I value. For each measurement, the corresponding pairs of I and I_0 are then substituted in equation (1) to calculate τ_{a632}.

[13] The transmissometer geometry was such that forward scattering had very minimal contribution. Indeed, the collimated beam, the small diameter of the transmission detector (3.2 mm), and a mechanical collimator (a 5 mm orifice in the front wall of the box, about 150 mm from the detector) minimized the effect of the forward scattering of the laser beam by the smoke aerosols. The average contribution of the forward scattering is estimated to come from a cone of less than ±0.1° around the center of the detector. Therefore, the forward scattering contribution to the transmitted beam was neglected in the AOT calculations.

2.4. Reliability of AOT Retrieval With the Transmissometer

[14] Since the transmissometer was a bespoke instrument conceived for this experiment, there is need to determine the reliability of its measurements before using the derived AOT values to estimate PM emissions. There was no direct way to validate the AOT measurements, but an indirect validation can be performed by correlating AOT with other aerosol measurements, such as $PM_{2.5}$ scattering coefficients at 632 nm ($\sigma_{sp(632)}$). To do that, the AOT values were first divided by the measurement optical path length (1.52 m) to convert them to extinction coefficients at 632 nm ($\sigma_{ep(632)}$), which are more compatible with $\sigma_{sp(632)}$. Also, since the two data sets had slightly different temporal resolutions, they were averaged at intervals of 10 s to render them temporally compatible as well.

[15] Figure 3 shows scatterplots of 10 s averages of $\sigma_{sp(632)}$ (nephelometer) against $\sigma_{ep(632)}$ (transmissometer), for fires 6D to 7E, which were the only fires for which both parameters were measured concurrently. The values were derived by spectral interpolation from the nephelometer measurements of $\sigma_{sp(550)}$ and $\sigma_{sp(700)}$, being $\sigma_{sp(632)} = \sigma_{sp(550)}/\mathrm{Exp}(-\alpha_{550/700} \times \ln(550/632))$, where $\alpha_{550/700} = -\ln(\sigma_{sp(550)}/\sigma_{sp(700)})/\ln(550/700)$ is the Ångstrom exponent, which is a measure of the particles' spectral dependence, indirectly expressing the particle size distribution, with smaller values ($\alpha < 1$) indicating a higher concentration of coarse (diameter > 2 μm) particles and vice versa [e.g., *Ichoku et al.*, 1999].

[16] Overall, there is a strong correlation between $\sigma_{sp(632)}$ and $\sigma_{ep(632)}$, with the least squares linear regression giving

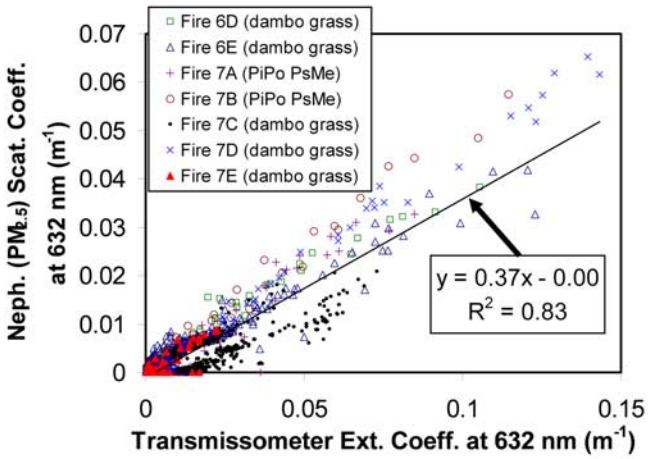

Figure 3. Scatterplots of scattering coefficients of $PM_{2.5}$ (particulate matter less than 2.5 μm aerodynamic diameter from the TSI 3563 nephelometer) against the extinction coefficients of total smoke aerosols (from the laser transmissometer). Individual points represent 10 s averages, and all data acquired throughout the duration of each fire are included. A least squares linear regression fitting performed on the entire data set produced a zero-intercept equation with an appreciably high r^2 value (as shown on the figure). Linear fits performed on individual fires also produced zero-intercept equations as follows: 6D ($y = 0.40x$ and $r^2 = 0.96$), 6E ($y = 0.35x$ and $r^2 = 0.83$), 7A ($y = 0.41x$ and $r^2 = 0.83$), 7B ($y = 0.49x$ and $r^2 = 0.98$), 7C ($y = 0.22x$ and $r^2 = 0.67$), 7D ($y = 0.46x$ and $r^2 = 0.99$), and 7E ($y = 0.42x$ and $r^2 = 0.88$).

zero intercept and $r^2 = 0.83$, which is statistically significant even at 0.001 probability level. The correlations were also good to excellent when fitted individually for each fire, as described in the Figure 3 caption. Although it is recognized that correlation is not necessarily a measure of absolute accuracy, in this case it indicates that the transmissometer has comparable sensitivity to variations in smoke particulate concentration as the nephelometer. The differences in the point scatter and slopes for the individual fires are probably due to differences in their emitted PM characteristics (scattering/absorption ratios), since the nephelometer measures only scattering and was limited only to $PM_{2.5}$ in this experiment. Note that the regression slope corresponds to single-scattering albedo (ω_0). However, the ω_0 values of $\sim$0.4 derived here are very low compared to typical literature values in the range of 0.6 to 0.97 for fresh smoke [e.g., *Reid et al.* 2005b]. This difference can probably be explained, partly by the fact that the nephelometer measurements were restricted to $PM_{2.5}$ while the transmissometer measured the total PM and partly by the fact that the smoke measured in this experiment was much fresher (a few seconds old) than what is typically measured in the field ($\sim$5 min up to 1 h old) as estimated in the work of *Reid et al.* [2005b]. In addition, on the basis of extensive literature analysis, *Reid et al.* [2005a] reported that in reality, the black carbon content of biomass-burning smoke has been known to vary from 2 to 30%, depending on fire chemistry, and at 30% black carbon by mass, ω_0 can drop to $\sim$0.4. Incidentally, the work of *Chen et al.* [2006] performed under the same conditions as those reported in this paper obtained an average ω_0 value of 0.32. In any case, the purpose of the scatterplot in Figure 3 was to show that the transmissometer measurement of AOT is reliable, at least to an extent comparable to that of the nephelometer.

3. Data Processing and Analysis

[17] The raw data measured during the experiment required some processing to calculate actual physical parameters relevant to the analysis performed here. The parameters that are important for this study are essentially the rates of biomass consumption and releases of FRE and PM (R_{BM}, R_{fre}, and R_{PM}, respectively). Sections 3.1, 3.2, and 3.3 summarize the processing performed to derive these parameters.

3.1. Rate of Biomass Consumption (R_{BM})

[18] Although the expected trend of the biomass measurement was that of a continuous decrease because of mass loss, the mass readings logged at intervals of 2 s fluctuated to some extent, because of air currents and thermal expansions/contractions of the burning table, such that a mass value was sometimes larger than one or more preceding values. To reduce the effect of this noise in calculating the burned biomass, the mass loss rate (R_{BM}) at a given time of measurement was obtained by subtracting the value measured at 10 intervals (approximately 20 s) before the current time from that measured at 10 intervals after and dividing the result by the total time interval between them (approximately 40 s). For instance, if $m_1, m_2, m_3, \ldots m_n$ denote the n mass readings logged from the scale at times $t_1, t_2, t_3, \ldots t_n$ during a given burn, then the mass loss rate at t_{50} is given by $R_{BM}^{(50)} = (m_{40} - m_{60})/(t_{40} - t_{60})$. The decision to calculate R_{BM} on the basis of $\pm$10 (rather than any other interval of) data points was based on overall visual assessment of the patterns of data fluctuation.

3.2. Rate of Release of Fire Radiative Energy (R_{fre})

[19] The raw data output by the Agema 550 thermal imager were infrared brightness temperatures at 3.9 μm per unit resolution cell (or pixel) of the 320 $\times$ 240 pixel thermal image. The data were acquired and saved every 1 s to a computer attached to the instrument, which viewed vertically downward onto each fire. Since these measurements were essentially monochromatic, the Planck function was used to calculate the pixel-level spectral radiances (in $W \times m^{-2} \times \mu m^{-1} \times sr^{-1}$), and a pixel was considered to contain fire if its spectral radiance exceeded 57.6 $W \times m^{-2} \times \mu m^{-1} \times sr^{-1}$ (or 477 K), which is close to the imager's detection limit (of 475 K), as described by *Wooster et al.* [2003, 2005] and *Freeborn et al.* [2008]. Using the midinfrared method developed by *Wooster et al.* [2003], the pixel radiances were converted to fire radiative power per pixel (in W). To convert flux density (i.e., $W\ m^{-2}$) to a radiant heat transfer rate (i.e., W), the line of sight distance between the sensor and the target was used to calculate the area of each pixel. The area of the pixel was assumed constant for every detector and parallel to the focal plane array. Values of all fire-

containing pixels in an image frame were summed to obtain the whole fire instantaneous FRP (or R_{fre}).

3.3. Rate of Emission of Smoke Particulate Matter (R_{PM})

[20] Each τ_{a632} value retrieved from the transmissometer measurements was used to calculate R_{PM} on the basis of an identical approach to that developed by *Ichoku and Kaufman* [2005] for use with MODIS satellite data products. First, τ_{a632} is converted to an aerosol column mass density (M_d g m^{-2}) using equation (2),

$$M_d = \frac{\tau_{a632}}{\beta_e}, \tag{2}$$

where β_e (expressed in m^2 g^{-1}) is the smoke aerosol specific extinction or mass extinction efficiency [e.g., *Chin et al.*, 2002]. *Ichoku and Kaufman* [2005] used a constant value of β_e = 4.6 m^2 g^{-1} at 550 nm wavelength based on values reported in the work of *Reid et al.* [2005b] from an extensive review of the published literature. Although β_e can be determined experimentally using measurements of AOT and PM mass concentration, this was not done in the current experiment because AOT measurements were time resolved, while the PM mass concentration was measured by collecting the PM samples on a single filter for an entire fire duration. Also, since calculation of β_e was not part of the experimental objectives, no prior effort was made to synchronize or even coordinate the start and end times of the two measurements. Furthermore, the filter samples were collected for $PM_{2.5}$ rather than for TPM, which the AOT refers to. *Reid et al.* [2005a] estimated that smoke $PM_{2.5}$ constitutes about 90% of TPM by mass. In any case, for consistency with the use of a constant β_e value in the method of *Ichoku and Kaufman* [2005], which is being evaluated in this study, as indicated in the objective expressed in section 1, a corresponding literature β_e value will be used here. Therefore, assuming β_e for smoke particles to be inversely proportional to wavelength at least at the typical visible to near-infrared aerosol measurement wavelengths [e.g., *Reid et al.*, 1998; *Chin et al.*, 2002], β_e = 4.4 m^2 g^{-1}, corresponding to the τ_a wavelength of 632 nm, was inferred from literature [*Reid et al.*, 2005b] and used in this experiment. β_e can increase with relative humidity (RH) because of aerosol hygroscopic growth. However, in a recent experiment conducted by *Chand et al.* [2005], by increasing RH from 15 to 90%, they found a very small (about 5%) relative increase in fresh smoke aerosol scattering (and by inference, β_e). In the current experiment, since the smoke was measured while still very fresh at an extremely low RH (the nephelometer recorded RH values <15% throughout the experiment), it was safe to assume that there was negligibly little to no RH effect.

[21] Aerosol particle mass concentration (C_m) per unit volume of air (in g m^{-3}) can be derived by dividing the column mass density (M_d) with the optical path length of measurement, assuming a homogeneous medium throughout the column, over a limited cross section. In typical aerosol measurements with Sun photometers, τ_a is measured vertically, but in this experiment, the column of τ_a measurement is the horizontal line between the transmissometer source and detector, as depicted in Figure 1. Therefore, the optical path length is equal to the stack diameter (D), and the smoke particulate mass concentration per unit volume (C_m g m^{-3}) is given by

$$C_m = \frac{M_d}{D}. \tag{3a}$$

[22] If the smoke stack airflow velocity measured with a hot-wire anemometer (see Table 1) is V m s^{-1} (see averages in Table 2, column 9), then the volumetric flow rate (R_v m^3 s^{-1}) with respect to the stack cross section is derived by multiplying V by the cross-sectional area of the stack ($\pi D^2/4$ m^2),

$$R_v = V \times \frac{\pi D^2}{4}. \tag{3b}$$

[23] Therefore, the mass flux or rate of emission of the smoke particulates (R_{PM}) is given by the product of the volume mass concentration (equation (3a)) and the volumetric flow rate (equation (3b)). Thus,

$$R_{PM} = \frac{M_d}{D} \times V \times \frac{\pi D^2}{4}, \tag{4}$$

where the units of expression for each of the variables in equation (4) are R_{PM} (g s^{-1}), M_d(g m^{-2}), V(m s^{-1}), and D (m).

4. Results

[24] To facilitate the joint analysis of data acquired with the different instruments, all time-resolved data sets were synchronized in time and subjected to temporal averaging at intervals of 10 s. Consequently, there was a reduction in data noise.

4.1. Characteristics of the Fires and Particulate Emissions

[25] Figure 4 shows a time series plot of R_{BM} and R_{fre}, as well as AOT and the emission ratio of CO to CO_2 (CO/CO_2) derived during the first fire in which the transmissometer was used (fire 6D). Figure 4 portrays the typical scenario of burn progression, fire radiative energy release, and smoke emission observed in most of the fires. As soon as the fire is ignited, the fuel loss becomes evident in the biomass measurement, and as the fire spreads across the fuel bed, the FRP becomes measurable and increases as flaming increases. Although not shown directly in this plot (to avoid clutter), the carbon dioxide (CO_2) emission curve tracks that of FRP during the flaming stage of the fire, and both reach their peak when the entire fuel bed is engulfed in flames. Since CO_2 is emitted predominantly during flaming, while CO emission greatly increases during smoldering (because of reduced combustion efficiency), the emission ratio of CO to CO_2 (i.e., CO/CO_2) is a good parameter to distinguish the flaming and smoldering stages of small fires such as those conducted in this experiment, with higher ratios indicating more smoldering [e.g., *Ward et al.*, 1991; *Chand et al.*, 2005]. The overall temporal characteristics of the biomass combustion and associated emissions during the current experiment are described in detail by *Freeborn et al.* [2008]. However, in a similar laboratory experiment, *Hungershofer et al.* [2004] observed that 0.08 or 8% CO/CO_2 emission ratio is a suitable

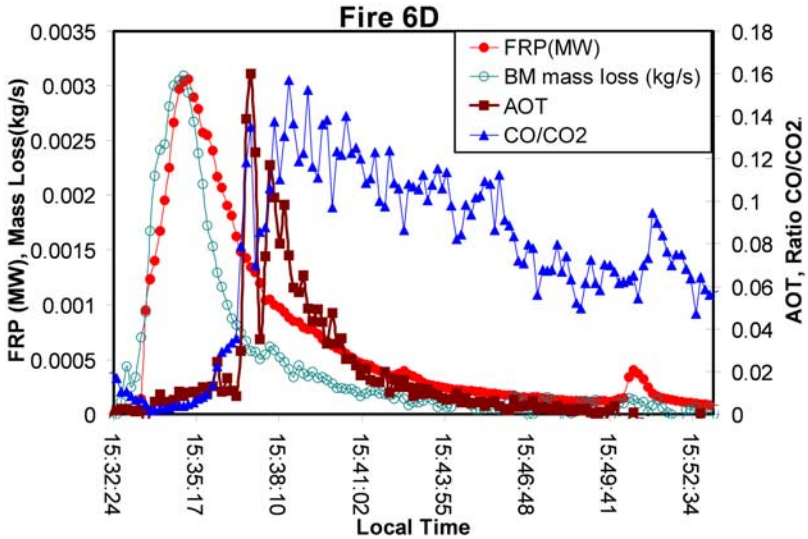

Figure 4. Time series of some essential parameters measured or derived during one of the experimental fires (6D) conducted with 0.57 kg of African dambo grass fuel. The curves represent fuel mass loss, FRP, AOT, and CO emission ratio (CO/CO_2).

threshold to separate flaming and smoldering emissions. In this experiment, for the dambo grass fires (6E, 6D, 7C, 7D, and 7E), Ångstrom exponent (α) was significantly different between flaming and smoldering, with a median value of 2.02 for flaming and 1.16 for smoldering, suggesting that the particles emitted during smoldering were larger. On the other hand, for the Pipo/PsMe fires (7A and 7B), there was no clear-cut distinction between flaming and smoldering, as they occurred more or less simultaneously (with an overall median α value of 1.9), probably because of inefficient combustion caused by the PsMe live foliage.

4.2. FRE-Based Particulate Emission Coefficients (C_e^{PM})

[26] *Ichoku and Kaufman* [2005] calculated the FRE-based particulate emission coefficients (C_e^{PM}) from slopes of zero-intercept linear least squares fits of a series of corresponding values of R_{fre} and R_{PM} derived from satellite measurements. In this experiment, R_{fre} and R_{PM} were derived as described in section 3 for all the fires conducted (with the exception of fires 8A and 8B, during which the transmissometer had a technical problem). Because of the necessary small size of these laboratory-scale fires, their flaming/smoldering/glowing stages are short lived and appreciably distinct from one another, and since R_{fre} peaks during the flaming phase and R_{PM} peaks during the smoldering phase, instantaneous measurements of R_{fre} and R_{PM} cannot be directly correlated (as the data of Figure 4 demonstrates). Therefore, for the condition of small laboratory-scale fires, it is not possible to derive a uniform C_e^{PM} from direct least squares fits of R_{fre} and R_{PM}. The relationship holds for landscape-scale fires as demonstrated by *Ichoku and Kaufman* [2005] because, at the spatial scale of the MODIS-derived data products (1 km for R_{fre} and 10 km for AOT), with few exceptions each satellite-measured pixel will contain a mix of all phases of the fire. The signature of these different phases are therefore integrated within both the R_{fre} and R_{PM} measures.

[27] To derive C_e^{PM} from the small-scale experimental fires conducted here, R_{fre} and R_{PM} were each integrated using time discrete summations over the entire duration of each fire to generate the total FRE and PM mass, respectively. The C_e^{PM} value for each individual fire is simply given by the ratio of PM to FRE as shown in Table 2 (column 12). However, the average C_e^{PM} for all the fires or groups of them can be derived by performing a zero-intercept linear least squares fit on a scatterplot of PM against FRE, such that

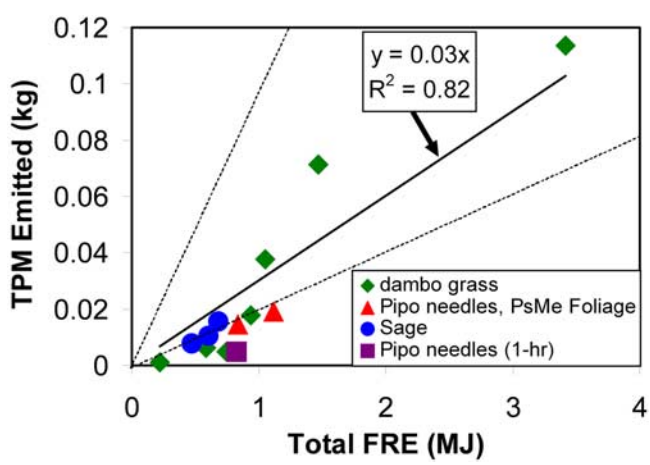

Figure 5. Scatterplot of total FRE against total emitted PM for the laboratory fires. Linear least squares fit with zero-intercept produced a slope of 0.03 kg MJ^{-1}, which represents the collective PM emission coefficient (C_e^{PM}) for the experiment. Separate regression fitting for dambo grass gave: ($y = 0.033x$ and $r^2 = 0.88$). The two dotted lines converging at the origin mark the range of the slopes generated from the different ecosystems in the satellite method [*Ichoku and Kaufman*, 2005].

$$\mathrm{PM} = C_e^{\mathrm{PM}} \times \mathrm{FRE}. \quad (5)$$

[28] Figure 5 shows the scatterplot, in which fires burned with the different fuel types are identified with different symbols. The zero-intercept linear fit on all data points produced a strong correlation (r^2 = 0.82) and an overall slope or C_e^{PM} value of 0.03 kg MJ^{-1}, which falls within the range derived from the equivalent spaceborne MODIS measurements [*Ichoku and Kaufman*, 2005], as delimited by the two dotted lines in Figure 5. A separate fit on the points representing the dambo grass fires alone gave C_e^{PM} = 0.033 and r^2 = 0.88. It is pertinent to mention that the smallest fires (with FRE < 1 MJ) tended to show lower PM values. This may be explained perhaps by the dissipation of a certain amount of smoke that could not enter the stack. Although this dissipated smoke may only constitute a small fraction of the smoke produced by the larger fires (FRE > 1 MJ), it may represent a significant fraction in the case of these smallest fires. Nevertheless, the points representing the sage and Pipo/PsMe fires appear to be aligned close to the 0.02 kg MJ^{-1} line, which incidentally was the value that *Ichoku and Kaufman* [2005] derived for North American boreal ecosystems where these vegetation types exist.

[29] To evaluate these results in the context of some other measurements and calculations performed in this experiment, Table 2 also shows for each fire biomass burned (column 7), FRE (column 8), and their ratio (column 10), which represents the combustion factor (F_c) derived by [*Wooster et al.*, 2005], whose value of 0.368 kg MJ^{-1}, derived from 29 mostly *Miscanthus* fires, falls within the range of those derived in this work. $PM_{2.5}$ total mass determined by gravimetric measurements of filter samples collected in each fire, as described by *Freeborn et al.* [2008], is listed in Table 2 (column 13) and has been used to calculate C_e^{PM} for $PM_{2.5}$ (column 14). As reported in the work of *Andreae and Merlet* [2001] on the basis of extensive literature review, given that the EF for $PM_{2.5}$ can be comparable to that of TPM for tropical forests or less by approximately 26, 35, and 70% for extratropical forests, savannas, and agricultural residues, respectively, it is encouraging that with only one exception (fire 7A), these values of C_e^{PM} for $PM_{2.5}$ obtained from filter analysis (Table 2, column 14) maintain acceptable proportions to those of the corresponding TPM based on transmissometer measurements (Table 2, column 12).

[30] It is pertinent to note that

$$\frac{C_e^x}{F_c} = \frac{M_x}{\mathrm{FRE}} \div \frac{M_{\mathrm{biomass}}}{\mathrm{FRE}} = \frac{M_x}{\mathrm{FRE}} \times \frac{\mathrm{FRE}}{M_{\mathrm{biomass}}} = \frac{M_x}{M_{\mathrm{biomass}}} = \mathrm{EF}_x, \quad (6)$$

where M_{biomass} is the mass of the biomass combusted, M_x is the mass of a given smoke species x (in this case $PM_{2.5}$ or TPM) emitted, and EF_x is its emission factor, as defined by *Andreae and Merlet* [2001, and references therein]. When equation (6) was implemented with the corresponding variables in Table 2, the computed values of EF_x (not shown) were often larger than the average literature values reported by *Andreae and Merlet* [2001] by a factor of 2 to 5, both for TPM and for $PM_{2.5}$. For instance, *Andreae and Merlet* [2001] reported the average literature values of EF($PM_{2.5}$) to be in the range of 3.9 to 13 g kg^{-1}, while those derived in this experiment are in the range of 3.5 to 36 g kg^{-1} [*Freeborn et al.*, 2008]. Note that *Andreae and Merlet* [2001] estimated the level of uncertainty of those literature values to be "at least" ±50%. Although the range of EF($PM_{2.5}$) values (4.8–12.1 g kg^{-1}) published by *Ottmar* [2001] agrees with those of *Andreae and Merlet* [2001], other authors have reported more variable ranges, notably 1.48–30.4 g kg^{-1} [*Yokelson et al.*, 1996] and 2.9–61.6 g kg^{-1} [*Christian et al.*, 2003]. Therefore, these literature values are unsuitable as a standard for evaluating the results obtained in this study.

[31] Naturally, the uncertainties in this work can originate from a number of different sources. *Wooster et al.* [2005] estimated the uncertainty in the methodology used in calculating FRP (i.e., R_{fre}) from thermal camera measurements, as performed in this work, to be about 12%. The maximum relative variation in the intensity measurement (represented by the vertical scatter in the nonsmoke segments of the transmissometer data in Figure 2b) is of the order of ±2%, although the absolute error is not known because the transmissometer was not absolutely calibrated. The assumed mass extinction efficiency value of β_e = 4.4 m^2 g^{-1} used to convert AOT to aerosol mass density was derived mostly from in situ measurements [*Reid et al.*, 2005b] and may not be appropriate for the laboratory-scale experiment done here. Furthermore, as discussed by *Ichoku and Kaufman* [2005], this β_e = 4.4 m^2 g^{-1} is about half of typical values used in emission modeling calculations [e.g., *Chin et al.*, 2002]. Added to this complexity, *Chen et al.* [2006] burned ponderosa pine wood and white pine needles in the same burning facility as for this study and obtained β_e values of 8.9 and 5 m^2 g^{-1}, respectively. Some uncertainty of unknown quantity may also have been incurred from the stack flow velocity measurements and the process of converting AOT to R_{PM}. Although it is not possible to identify all error sources and quantify them from the measurements performed in this experiment, considering the foregoing factors, it is roughly estimated that the uncertainty in the C_e^{PM}determined here would be of the order of ±50%.

5. Conclusions

[32] A series of laboratory-scale fires conducted in a combustion chamber have provided further insight into the characteristics of fires and the relationship between fire strength and smoke aerosol (PM) emission. At such an elementary scale, it is easier to observe the three distinct stages of fires, flaming, smoldering, and glowing, which exhibit different intensities of biomass consumption and release of energy and emissions. Typically, biomass is consumed most rapidly during the flaming phase, which is highly energetic with efficient combustion, and FRE and CO_2 are released with great intensity. After flaming has reached its peak, both the upper layer of fuel and the surrounding oxygen supply are used up and flaming, and FRE and CO_2 quickly decline, giving way to smoldering, which slowly burns the fuel beneath with less efficiency, releasing high concentrations of CO and PM. As the biomass fuel is depleted, smoldering subsides, and glowing takes effect, releasing less and less radiative energy and smoke until the fire dies completely.

[33] One of the outcomes of this research is that a simple laser transmissometer can be used in an experimental setting to measure smoke light transmittance from which AOT can be derived to an appreciable level of reliability. This has enabled us to simulate in the laboratory the measurement of AOT from satellites, in order to implement satellite-like smoke emissions estimations in a controlled environment. The transmissometer-derived particulate extinction coefficient $\sigma_{ep(632)}$ showed a strong correlation ($r^2 = 0.83$) with scattering coefficient $\sigma_{sp(632)}$ measured with a nephelometer. AOTs measured with the transmissometer were used to derive the smoke PM emission rate (R_{PM}), which has never been measured before in this way, in a laboratory setting. Incidentally, at such limited fire scale, there is no real-time correlation between R_{fre} and R_{PM}, because the former is strongest during flaming while the latter is strongest during smoldering. However, when R_{fre} and R_{PM} are integrated in time for the fire duration, whereby all stages of the fire are well represented in the parameters, the corresponding total FRE and PM show a very good correlation, allowing the derivation of PM emission coefficient (C_e^{PM}).

[34] An interesting aspect of this study is the scale and scalability of the laboratory measurements, especially with respect to particulate matter. The average C_e^{PM} value of 0.03 kg MJ^{-1} derived in this laboratory experiment agrees with those derived from satellite measurements [*Ichoku and Kaufman*, 2005]. This close agreement in PM emission coefficient (C_e^{PM}) between laboratory and satellite measurements is a major breakthrough in the validation of emissions from satellite measurements of FRE. Although this is not a direct validation, nevertheless, since similar values were obtained without imposing any boundary constraints, it provides a general basis of validity to pursue research in this domain. The main accomplishment at this stage of the research is not on whether high absolute accuracies have been achieved. Rather, it is the establishment of the proof of concept that the technique for direct estimates of emissions based on satellite R_{fre} and AOT measurements [*Ichoku and Kaufman*, 2005] can be imitated in the laboratory. Future efforts shall be devoted to employing very well calibrated instruments and conducting large numbers of burns with a very large variety of biomass types, with the hope of achieving resounding success in characterizing the process sufficiently for improving and validating direct emissions estimates from satellite-based R_{fre} measurements. The potential benefits of such success will be far reaching, providing opportunities for a great diversity of applications, including for fire disaster containment, air quality, health, environmental sanitation, weather, and climate.

[35] **Acknowledgments.** We appreciate the efforts of Amer Rahabi for his assistance in building the laser transmissometer. We also thank the staff of the U.S. Forest Service Fire Sciences Laboratory (FiSL), particularly Michael Chandler, Cyle Wold, Emily Lincoln, Penny Bertram, and Danne Guthrie for their support and help during the experiment. Martin Wooster's participation in this research was supported primarily by NERC grant NERC NE/C520712/1.

References

Andreae, M. O., and P. Merlet (2001), Emission of trace gases and aerosols from biomass burning, *Global Biogeochem. Cycles*, *15*, 955–995, doi:10.1029/2000GB001382.

Chand, D., O. Schmid, P. Gwaze, R. S. Parmar, G. Helas, K. Zeromskiene, A. Wiedensohler, A. Massling, and M. O. Andreae (2005), Laboratory measurements of smoke optical properties from the burning of Indonesian peat and other types of biomass, *Geophys. Res. Lett.*, *32*, L12819, doi:10.1029/2005GL022678.

Chen, L.-W. A., H. Moosmüller, W. P. Arnott, J. C. Chow, J. G. Watson, R. A. Susott, R. E. Babbitt, C. E. Wold, E. N. Lincoln, and W. M. Hao (2006), Particle emissions from laboratory combustion of wildland fuels: In situ optical and mass measurements, *Geophys. Res. Lett.*, *33*, L04803, doi:10.1029/2005GL024838.

Chin, M., P. Ginoux, S. Kinne, O. Torres, B. N. Holben, B. N. Duncan, R. V. Martin, J. A. Logan, A. Higurashi, and T. Nakajima (2002), Tropospheric aerosol optical thickness from the GOCART model and comparisons with satellite and Sun photometer measurements, *J. Atmos. Sci.*, *59*, 461–483, doi:10.1175/1520-0469(2002)059<0461:TAOTFT>2.0.CO;2.

Christian, T. J., B. Kleiss, R. J. Yokelson, R. Holzinger, P. J. Crutzen, W. M. Hao, B. H. Saharjo, and D. E. Ward (2003), Comprehensive laboratory measurements of biomass-burning emissions: 1. Emissions from Indonesian, African, and other fuels, *J. Geophys. Res.*, *10*(D23), 4719, doi:10.1029/2003JD003704.

Crutzen, P. J., and M. O. Andreae (1990), Biomass burning in the tropics: Impact on atmospheric chemistry and biogeochemical cycles, *Science*, *250*, 1669–1678, doi:10.1126/science.250.4988.1669.

Crutzen, P. J., L. E. Heidt, J. P. Krasnec, W. H. Pollock, and W. Seiler (1979), Biomass burning as a source of atmospheric gases CO, H_2, N_2O, NO, CH_3Cl and COS, *Nature*, *282*, 253–255, doi:10.1038/282253a0.

DeBell, L. J., R. W. Talbot, J. E. Dibb, J. W. Munger, E. V. Fischer, and S. E. Frolking (2004), A major regional air pollution event in the northeastern United States caused by extensive forest fires in Quebec, Canada, *J. Geophys. Res.*, *109*, D19305, doi:10.1029/2004JD004840.

Feingold, G., H. Jiang, and J. Y. Harrington (2005), On smoke suppression of clouds in Amazonia, *Geophys. Res. Lett.*, *32*, L02804, doi:10.1029/2004GL021369.

Freeborn, P. H., M. J. Wooster, W. M. Hao, C. A. Ryan, B. L. Nordgren, S. P. Baker, and C. Ichoku (2008), Relationships between energy release, fuel mass loss, and trace gas and aerosol emissions during laboratory biomass fires, *J. Geophys. Res.*, *113*, D01301, doi:10.1029/2007JD008679.

Fuller, D. O. (2000), Satellite remote sensing of biomass burning with optical and thermal sensors, *Prog. Phys. Geogr.*, *24*(4), 543–561.

Hao, W. M., and M.-H. Liu (1994), Spatial and temporal distribution of tropical biomass burning, *Global Biogeochem. Cycles*, *8*, 495–503, doi:10.1029/94GB02086.

Hungershofer, K., et al. (2004), Optical properties of particles from laboratory fires: Comparison between measurements and Mie calculations, in *Proceedings of the International Radiation Symposium (IRS)*, edited by H. Fischer and B.-J. Sohn, A. Deepak, Hampton, Va.

Ichoku, C., and Y. J. Kaufman (2005), A method to derive smoke emission rates from MODIS fire radiative energy measurements, *IEEE Trans. Geosci. Remote Sens.*, *43*(11), 2636–2649, doi:10.1109/TGRS.2005.857328.

Ichoku, C., et al. (1999), Interrelationships between aerosol characteristics and light scattering during late winter in an eastern Mediterranean arid environment, *J. Geophys. Res.*, *104*, 24,371–24,393, doi:10.1029/1999JD900781.

Kaufman, Y. J., L. A. Remer, R. Ottmar, D. Ward, R.-R. Li, R. Kleidman, R. Fraser, L. Flynn, D. McDougal, and G. Shelton (1996), Relationship between remotely sensed fire intensity and rate of emission of smoke: SCAR-C experiment, in *Global Biomass Burning*, edited by J. Levine, pp. 685–696, MIT Press, Cambridge, Mass.

Kaufman, Y. J., C. O. Justice, L. P. Flynn, J. D. Kendall, E. M. Prins, L. Giglio, D. E. Ward, W. P. Menzel, and A. W. Setzer (1998), Potential global fire monitoring from EOS-MODIS, *J. Geophys. Res.*, *103*, 32,215–32,238, doi:10.1029/98JD01644.

Koren, I., Y. J. Kaufman, L. A. Remer, and J. V. Martins (2004), Measurement of the effect of Amazon smoke on inhibition of cloud formation, *Science*, *303*, 1342–1345, doi:10.1126/science.1089424.

Kulkarni, N. S., B. Prudon, S. L. Panditi, Y. Abebe, and J. Grigg (2005), Carbon loading of alveolar macrophages in adults and children exposed to biomass smoke particles, *Sci. Total Environ.*, *345*(1–3), 23–30, doi:10.1016/j.scitotenv.2004.10.016.

Liu, Y. Q. (2005), Atmospheric response and feedback to radiative forcing from biomass burning in tropical South America, *Agric. For. Meteorol.*, *133*(1–4), 40–53, doi:10.1016/j.agrformet.2005.03.011.

McMeeking, G. R., et al. (2006), Smoke-impacted regional haze in California during the summer of 2002, *Agric. For. Meteorol.*, *137*(1–2), 25–42, doi:10.1016/j.agrformet.2006.01.011.

Ottmar, C. C. (2001), Smoke source characteristics, in *Smoke Management Guide for Prescribed and Wildland Fire*, edited by C. C. Hardy et al., *PMS 420-2*, 226 pp., Natl. Wildfire Coord. Group, Boise, Idaho.

Procopio, A. S., P. Artaxo, Y. J. Kaufman, L. A. Remer, J. S. Schafer, and B. N. Holben (2004), Multiyear analysis of Amazonian biomass burning

smoke radiative forcing of climate, *Geophys. Res. Lett.*, *31*, L03108, doi:10.1029/2003GL018646.

Reid, J. S., P. V. Hobbs, R. J. Ferek, D. R. Blake, J. V. Martins, M. R. Dunlap, and C. Liousse (1998), Physical, chemical, and optical properties of regional hazes dominated by smoke in Brazil, *J. Geophys. Res.*, *103*, 32,059–32,080, doi:10.1029/98JD00458.

Reid, J. S., R. Koppmann, T. F. Eck, and D. P. Eleuterio (2005a), A review of biomass burning emissions, part II: Intensive physical properties of biomass burning particles, *Atmos. Chem. Phys.*, *5*, 799–825.

Reid, J. S., T. F. Eck, S. A. Christopher, R. Koppmann, O. Dubovik, D. P. Eleuterio, B. N. Holben, E. A. Reid, and J. Zhang (2005b), A review of biomass burning emissions, part III: Intensive optical properties of biomass burning particles, *Atmos. Chem. Phys.*, *5*, 827–849.

Roberts, G., M. J. Wooster, G. L. W. Perry, N. Drake, L.-M. Rebelo, and F. Dipotso (2005), Retrieval of biomass combustion rates and totals from fire radiative power observations: Application to southern Africa using geostationary SEVIRI imagery, *J. Geophys. Res.*, *110*, D21111, doi:10.1029/2005JD006018.

Seiler, W., and P. J. Crutzen (1980), Estimates of gross and net fluxes of carbon between the biosphere and the atmosphere from biomass burning, *Clim. Change*, *2*, 207–248, doi:10.1007/BF00137988.

Ward, D. E., A. W. Setzer, Y. J. Kaufman, and R. A. Rasmussen (1991), Characteristics of smoke emission from biomass fires of the Amazon region–Base-A experiment, in *Global Biomass Burning: Atmospheric, Climatic, and Biospheric Implications*, edited by J. S. Levine, pp. 394–401, MIT Press, Cambridge, Mass.

Wooster, M. J. (2002), Small-scale experimental testing of fire radiative energy for quantifying mass combusted in natural vegetation fires, *Geophys. Res. Lett.*, *29*(21), 2027, doi:10.1029/2002GL015487.

Wooster, M. J., B. Zhukov, and D. Oertel (2003), Fire radiative energy for quantitative study of biomass burning: Derivation from the BIRD experimental satellite and comparison to MODIS fire products, *Remote Sens. Environ.*, *86*, 83–107, doi:10.1016/S0034-4257(03)00070-1.

Wooster, M. J., G. Perry, B. Zukov, and D. Oertel (2004), Biomass burning emissions inventories: Modelling and remote sensing of fire intensity and biomass combustion rates, in *Spatial Modelling of the Terrestrial Environment*, edited by R. Kelly, N. Drake, and S. Barr, pp. 175–196, John Wiley, Hoboken, N. J.

Wooster, M. J., G. Roberts, G. L. W. Perry, and Y. J. Kaufman (2005), Retrieval of biomass combustion rates and totals from fire radiative power observations: FRP derivation and calibration relationships between biomass consumption and fire radiative energy release, *J. Geophys. Res.*, *110*, D24311, doi:10.1029/2005JD006318.

Wu, J., A. M. Winer, and R. J. Delfino (2006), Exposure assessment of particulate matter air pollution before, during, and after the 2003 southern California wildfires, *Atmos. Environ.*, *40*(18), 3333–3348, doi:10.1016/j.atmosenv.2006.01.056.

Yokelson, R. J., D. W. T. Griffith, J. B. Burkholder, and D. E. Ward (1996), Open-path Fourier transform infrared studies of large-scale laboratory biomass fires, *J. Geophys. Res.*, *101*, 21,067–21,080, doi:10.1029/96JD01800.

S. Baker, W. M. Hao, B. L. Nordgren, and C. A. Ryan, Fire Sciences Laboratory, Rocky Mountain Research Station, USDA Forest Service, P.O. Box 8089, Missoula, MT 59808, USA.

P. H. Freeborn and M. J. Wooster, Department of Geography, King's College London, Strand, London, WC2R 2 LS, UK.

C. Ichoku, Climate and Radiation Branch, NASA Goddard Space Flight Center, Code 913, Building 33, Greenbelt, MD 20771, USA. (ichoku@climate.gsfc.nasa.gov)

J. V. Martins, Department of Physics, University of Maryland, Baltimore County, Baltimore, MD 21250, USA.